

Deep learning techniques applied to the physics of extensive air showers

A. Guillén^a, A. Bueno^b, J. M. Carceller^b, J. C. Martínez-Velázquez^b, G. Rubio^b, C. J. Todero Peixoto^{b,c}, P. Sanchez-Lucas^{b,1}

^a*Dpto. de Arquitectura y Tecnología de Computadores, Universidad de Granada, Granada, Spain.*

^b*Dpto. de Física Teórica y del Cosmos & C.A.F.P.E., Universidad de Granada, Granada.*

^c*Depto. de Ciências Básicas e Ambientais, Escola de Engenharia de Lorena, U. of São Paulo, São Paulo, Brazil.*

Abstract

Deep neural networks are a powerful technique that have found ample applications in several branches of Physics. In this work, we apply machine learning algorithms to a specific problem of Cosmic Ray Physics: the estimation of the muon content of extensive air showers when measured at the ground. As a working case, we explore the performance of a deep neural network applied to the signals recorded by the water-Cherenkov detectors of the Surface Detector Array of the Pierre Auger Observatory. We apply deep learning architectures to large sets of simulated data. The inner structure of the neural network is optimized through the use of genetic algorithms. To obtain a prediction of the recorded muon signal in each individual detector, we train neural networks with a mixed sample of light, intermediate and heavy nuclei. When true and predicted signals are compared at detector level, the primary values of the Pearson correlation coefficients are above 95%. The relative errors of the predicted muon signals are below 10% and do not depend on the event energy, zenith angle, total signal size, distance range or the hadronic model used to generate the events.

Keywords: machine learning, deep neural networks, ultra-high energy, cosmic rays, Pierre Auger Observatory

1. Introduction

Ultra-high energy cosmic rays (UHECR) are atomic nuclei with energies above 10^{18} eV. They constitute the most energetic form of radiation ever detected by humankind. Note that, when expressed in a reference frame where one of the protons is at rest, the energy of the proton beam accelerated at LHC in its present configuration reaches 10^{17} eV. UHECR were discovered

¹now at U. of Zürich

more than 50 years ago [1]. However, we still lack a plausible theory that explains the chemical composition of this radiation, where it is produced and what mechanisms are capable of conferring to these nuclei such extraordinary energies. We know that their flux is a steeply decreasing function of energy. For example, for energies above 10^{19} eV, we detect on average one particle per km^2 per year. This fact prevents us from detecting directly the primary particle. Thus the only way left to study the properties of UHECR is through the analysis of the extensive air showers produced after UHECR collide with the nuclei of the Earth's atmosphere.

The Pierre Auger Observatory is the biggest instrument built so far to scrutinize the mysteries of UHECR [2]. It works in the so-called *hybrid mode* since it is able to measure with fluorescence telescopes the light produced by the de-excitation of the atmospheric nitrogen and it samples as well the particles of the air-shower that reach the ground with an array of water-Cherenkov detectors, covering a surface of 3000 km^2 . The latter is known as the Surface Detector (SD). The signals recorded by the surface stations is a mix of two kinds of particles: electromagnetic (photons, electrons and positrons) and (anti)muons. The construction of the Pierre Auger Observatory was completed in 2008, but it has been taking data steadily since 2004 for a total accumulated exposure that nowadays is above $10^5 \text{ km}^2 \text{ sr year}$. This is the largest data sample ever collected in this field of Physics to advance our understanding of the properties of the non-thermal Universe.

The SD is not optimized to separate in a clean way the signals produced by the muons traversing it from those produced by the electromagnetic component. The measurement of the muon signal is of the utmost importance to understand how well models of hadronic interactions describe the data [3, 4]. It is also key to perform an analysis of the mass composition of the primary flux of UHECR on an event-by-event basis. This kind of analysis might open the door to solving the mystery of where UHECR are produced and what is the origin of the observed flux suppression at extreme energies. The prospects for enhanced mass composition analyses and the observed mismatch in the number of muons between data and simulations are the main motivations behind the upgrade of the Auger Observatory, dubbed AugerPrime [5].

Recently the Telescope Array collaboration has also reported an excess of signals with large muon purity when compared to predictions from simulations [6]. Therefore, given its importance, it comes as no surprise that the problem of estimating the muon content of extensive air showers at the ground had been tackled in several ways by different collaborations. For example, AugerPrime proposes a solution based on instrumentation: each water-Cherenkov detector is equipped with a complementary plastic scintillator detector on top of it. This new detector is mostly sensitive to the electromagnetic component of the extensive air-shower. Therefore it is through the combination of the two signals, simultaneously registered by each enhanced station, that the muon signal is obtained. The matrix formalism to be employed to extract the muon contribution is similar to the one proposed in [7].

Focusing on the particular case of the Pierre Auger Observatory, we discuss

here a new complementary approach to estimate the amount of muonic signal. It is a software solution based on the use of deep learning algorithms [8, 9]. We have used Monte Carlo events originated by primaries of several species. They have been fully simulated and reconstructed using the official software of the Pierre Auger Collaboration [10]. With them we assess the performance of this new method in the energy range where the Auger SD is fully efficient.

2. Deep Neural Networks: design and training

Neural networks are loosely based on human neural networks. In those, neurons are interconnected and the information is transmitted through these connections. In Artificial or Deep Neural Networks (DNN), each neuron computes a function of a linear combination of its inputs: the *activation function*. The input of this function can be the data that we feed the neural net with or the output of other neurons. The output of this function can then be used by other neurons. See the left panel of Figure 1.

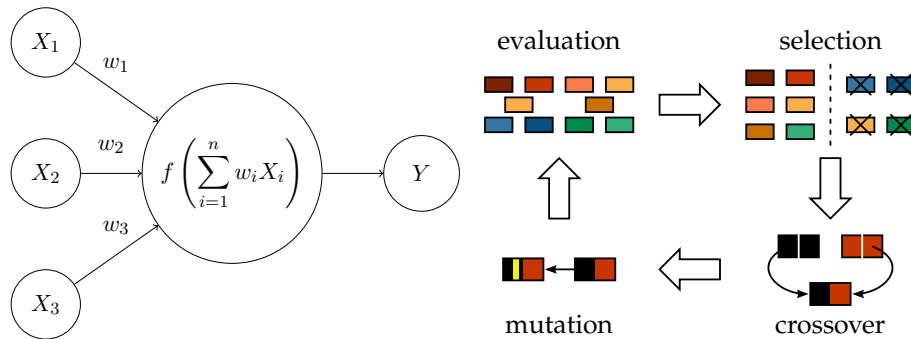


Figure 1: (Left) Example of a single neuron with three inputs: X_i . The three weights w_j are free parameters and will be adjusted during the training process. The neuron computes an activation function f that gives an output Y . (Right) Diagram of the genetic algorithm used in this work. Neural networks are built with random structures and trained. The networks with better performance are selected in binary tournaments. Only for the selected networks, we cross the number of neurons in some layers between individuals and we introduce mutations (change randomly the numbers of neurons in certain layers). This process provides a new generation of networks ready to be trained.

Neurons are grouped in layers, with the first layer being the input layer, the last one being the output layer and those in the middle are called hidden layers. In this work we use supervised learning. Therefore, in the first stage, the neural net is trained on labelled data: the predictions of the neural net and the true values are compared, and the error is minimized. This is done by changing the weights in the linear combinations that make up the input of each neuron.

In the following subsections, the technical aspects of the neural net that we have built are explained. There are several possible choices when building a neural network: the number of neurons in each layer, the number of layers,

the activation function, etc. We explain the process followed to chose these hyperparameters, and in the end, we give an overview of the final architecture of the neural network that we used. The code has been implemented using the functions provided by the SciPy ecosystem [11] (numpy and matplotlib), scikit-learn [12] and keras [13] using tensorflow [14], all interpreted by Python (version 3.6).

2.1. Data preprocessing

Following the recommendations in [15], the data used as input and the output (muon signal) have been normalized each one independently with mean $\mu = 0$ and standard deviation $\sigma = 1$. Before normalizing, some variables have been transformed to help the neural network learn. The details are explained in Section 3.

2.2. Activation function and weight initialization

Each neuron computes a function of the linear combination of its inputs, and its output is connected to other neurons in subsequent layers. There is a wide variety of functions that can be chosen, although, following the recommendations in [16, 17], the Rectifier Linear unit (ReLu, defined as $f(x) = \max\{0, x\}$) could be the best choice. Nonetheless, instead of choosing it ourselves, we have let the genetic algorithm chose the one that gave the best performance.

Regarding the initialization of the weights of the neural network, after analysing different methods, we have obtained the bests results using a random weight initialization that takes values from a normal distribution with mean $\mu = 0$ and standard deviation $\sigma = 0.05$.

2.3. Optimization algorithm and loss function

During the training process, the weights in the connections between each layer have to be optimized. To do so, it is necessary to define a loss function, that is, a function that measures how well the neural net is predicting its output. As we are dealing with a regression problem and no other restrictions are known, one reasonable criterion to determine if the model has a good performance is the mean squared error (MSE):

$$\text{MSE} = \frac{1}{n} \sum_{i=1}^n (Y_{\text{true}}^{(i)} - Y_{\text{pred}}^{(i)})^2 \quad (1)$$

where n is the number of samples, $Y_{\text{true}}^{(i)}$ is the true value that we want to predict for the i -th example and $Y_{\text{pred}}^{(i)}$ is the prediction done by the neural network for the same example. This is the function that will be minimized during the training process.

The optimization algorithm used was the Adam (Adaptative momentum) [18] which is a stochastic gradient-based method. The gradients are computed and then corrected using a first and second raw moment estimate, leading to the new value of the parameters to be optimized.

2.4. Genetic algorithm

Genetic Algorithms (GAs) are global optimization algorithms that have been widely used in many areas where there is no better way of doing things than trying random numbers. The idea beneath these algorithms is to imitate the behaviour of nature by evolving populations of individuals through time, in a way that only the best ones last, see the right panel of Figure 1. We have let the width (number of neurons in each layer), depth (number of layers) and choice of activation function free for the genetic algorithm to pick the best combination.

The first step is to decide what to choose as the individual that will be evolved over time. For the sake of simplicity, we have defined our DNN as a vector of a certain length, whose elements are a natural number in the interval $[0, 100]$. This set of natural numbers corresponds to the number of neurons in each layer. This vector also has an integer that maps the type of activation function, and therefore, the algorithm can check different combinations of them.

We generated randomly 50 individuals, or 50 neural networks with random number of neurons in each layer, random number of layers and random activation functions. We have repeated the following process for 100 iterations. To compute the fitness of each individual, networks are trained over ten epochs to have an estimation of their potential performance. Once they are evaluated, a binary tournament selection is carried out to obtain the subset of individuals that are the ancestors for the generation of the offspring. Then there is a two-point crossover, that is, the number of neurons in each layer from a certain start layer l_0 up to an end layer l_1 are exchanged between two individuals with probability 0.8. The last step is to mutate or change randomly, with probability 0.1, the number of neurons in each layer of an individual. When the new population is available, we have used an elitism mechanism where the best individual in the current population is included into the next one.

A filter was also applied. When any layer was found to have less than five neurons, it was discarded. In this way, we make sure that the layer is really needed and there is no need to “dropout” or apply regularisation afterwards. The last layer only has one neuron and is used to obtain the output.

2.5. Final DNN structure

The final DNN obtained is represented in Figure 2. The network is made up of six layers: five fully connected layers using ReLu as activation function and a final layer that combines the outputs from the fifth layer linearly. In this neural net, complexity starts increasing from low to high (from 9 to 56 neurons) and then it decreases drastically to the point where it started. The reason why the number of layers is equal to six is that the first runs of the GA using a maximum of ten layers always decreased the number of them to six or seven. So we executed the GA again (with a maximum number of layers set to six) obtaining the current configuration. In this way, once we

explored complex solutions regarding the network depth, we exploited the reduced solution space to determine more precisely how many neurons per layer should be included.

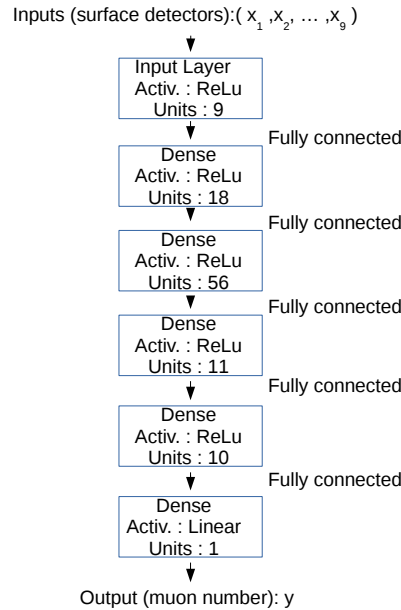


Figure 2: Final structure of the NN used for the experiments. It has five fully connected layers using ReLu as activation function. The numbers of neurons in each layer are indicated.

3. Application to the problem of measuring the muon signal recorded by the water-Cherenkov detectors of the Pierre Auger Observatory

The Surface Array of the Auger Observatory consists of 1660 water-Cherenkov detectors laid out in a triangular grid, whose separation between closest-neighbours is 1500 m. These detectors provide the arrival times of the particles that impinge on them. Each detector is equipped with three PMTs, the signals registered by them are digitized by 40 MHz 10-bit Flash Analog to Digital Converters (FADCs). For each triggered station, $19.2 \mu\text{s}$ (768 bins of 25 ns each) of data are recorded by every FADC. The signals are expressed in units of VEM [19]. A VEM (“Vertical Equivalent Muon”) is the total signal left by a muon that traverses the water-Cherenkov detector vertically at its center. Figure 3 shows two examples of typical FADC traces.

As stated before, the FADC traces are a mix of the electromagnetic and muonic components present in extensive air showers. To fully exploit the Physics information encoded in the signals recorded by the water-Cherenkov detectors, it is a must to separate the contributions of the different particle

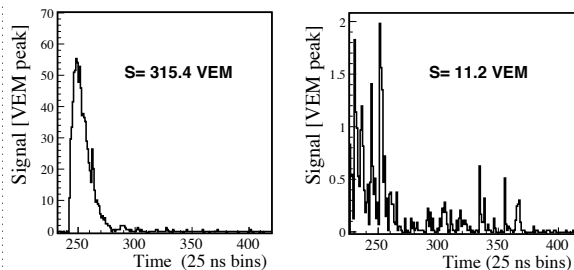


Figure 3: FADC traces corresponding to triggered detectors located at 650 (left) and 1780 (right) m from the reconstructed core of an extensive air-shower. The traces, corresponding to a typical vertical event of 3×10^{19} eV, are mix of electromagnetic and muonic particles. The spiky structure is attributed to be caused mainly by muons, while the accumulations of signals left by photons or electrons/positrons are usually more spread in time. These traces are reproduced from [2].

species that traverse the stations. Therefore, the goal of this study is to estimate, for every single triggered detector used in the reconstruction of an event, the amount of signal that corresponds to the energy deposited by muons. We do not work with events whose energy lies below 3×10^{18} eV since this is the minimum energy at which the Auger trigger efficiency reaches 100% for the events recorded by the 1500 m array. In this way, we avoid applying correction factors associated with trigger inefficiencies.

We feed the neural network with the set of variables described below. Notice that some of them pertain to the global features of the event (items 1 and 2 in the list below), others refer specifically to the information furnished at station level. The observables chosen to provide information at station level are those customarily used in the Physics analyses of the Pierre Auger collaboration [20]. The total trace used in our analysis is computed as the average of the traces recorded by each of the active PMTs of a station. In our analysis, we do not use detectors with signs of saturated traces. We disregard as well stations whose measured total signal is below 10 VEM (above this value the probability of single detector triggering is close to 100%). The chosen list of variables read as follows:

1. True Monte Carlo energy. We use as input variable the decimal logarithm of energy, which is measured in eV.
2. Zenith angle: θ . It is measured in degrees. For this study and due to the lack of simulated horizontal events, we limit ourselves to angles below 45 degrees².
3. Distance of the station to the reconstructed core of the air-shower. We measure it in meters.
4. Total signal registered by the station. We measure it in VEMs.

²In principle, we cannot think of any showstopper that prevents us from applying the same kind of treatment to more horizontal events.

5. Trace length. Number of 25 ns bins between the Start and End bins of the trace.
6. Azimuthal angle of the detector. It is measured in radians.
7. Risetime, $t_{1/2}$ (computed as discussed in [21]). The risetime is defined as the time it takes for the integrated signal to grow from 10% up to 50% of its total value and it is measured in ns.
8. Falltime (computed following [21]). Time for the integrated signal to go from 50% to 90% of its total value and it is measured in ns.
9. Area over Peak. It is defined as the ratio of the integral of the FADC trace to its peak value.
10. The true value of the total muonic signal S_{μ}^{true} , measured in VEMs. This is the output value of the learning process and it is obviously not used to train the neural network. It is simply used as a reference to guide the whole process.

This set of mixed global and local (station level) variables performs well. Enlarging it with new observables to obtain a better estimation of the muon signal does not significantly improve our results. In particular, one can think that feeding the net with the whole temporal series of bins that form the trace would substantially improve the precision with which the muon signal is extracted. We observed that in that case the gain is almost negligible, while the computational cost in terms of time increases by a sizeable factor.

We decided to train the network with events generated using the QGSJETII-04 model [22]. The events have been generated with a distribution that is uniform in energy. Once the internal network architecture is fixed and its performance evaluated with QGSJETII-04 events, we use EPOS-LHC [23] to show how our results depend on the different assumptions made to model hadronic interactions at ultra-high energies. Another vital decision is related to the nature of the nucleus (or set of nuclei) used to train the neural network. We observed that training the network with a single species is a far from optimal decision. For example, when iron nuclei are used to build the network, the number of predicted muons in events generated by protons is grossly underestimated. While the Pearson correlation coefficient between the true and estimated muon signals is 94% for a fresh sample of iron nuclei, it drops below 80% when protons are used as the validation sample. Similar conclusions are drawn when a pure sample of protons is used to train the network and, later, we assess its performance on iron nuclei. Since protons and iron nuclei differ in the values of the local variables for fixed values of the energy and zenith angle, the use of a single species to define the internal structure of the network does not guarantee an efficient coverage of the full available phase space of possible configurations. The situation improves when the network is trained with a mix of iron nuclei and protons in equal amounts. However, we observed that our estimations of the muonic signal improve even more when a mix of equal fractions of proton, helium, nitrogen and iron nuclei is used in the final training sample.

As a recapitulation, Table 1 shows the numbers of events generated and the stations used to train, test and validate the deep neural networks algorithms for two models of hadronic interactions. The events have been simulated using the CORSIKA package version 74004 [24] and reconstructed using an official version of `Offline` (i.e., the Auger simulation and reconstruction software [10]).

Table 1: Summary of the simulated events and detectors used in this work. Notice that the batches of stations used for training, validation and test correspond to distinct sets of detectors.

QGSJETII-04				
		Training	Validation	Test
Primary	# of events	# of detectors		
Proton	19362	16088	4022	57522
Helium	12341	15960	3989	36740
Nitrogen	12201	16071	4017	36069
Iron	19478	16076	4018	65455
EPOS-LHC				
		Training	Validation	Test
Primary	# of events	# of detectors		
Proton	18456	–	–	78063
Iron	18779	–	–	86862

4. Results

We use the following conventions in the ensuing plots: proton primaries are represented by red solid circles; He by brown open circles; N corresponds to orange open triangles and finally Fe is represented as blue solid squares. Once the inner architecture of the neural net has been defined, following the procedures outlined in Section 3, we show to it fresh samples of nuclei generated with QGSJETII-04 and EPOS-LHC models. The discussion of the outcome of this procedure follows.

4.1. QGSJETII-04 simulations: results at detector level

Figure 4 shows, in units of VEM, the distribution of muonic signals for a set of events generated with QGSJETII-04. They have energies higher than $10^{18.5}$ eV and zenith angles up to 45 degrees. We consider stations with total measured signals above 10 VEM. The figures in this section show results at the single station level. The top panels illustrate the true muonic signal for the four considered species. The four bottom panels show the distributions of predicted muonic signals. The similarities with the true distributions are striking. This is illustrated in Figure 5 where the difference between true and predicted signals is plotted for every nuclei. We obtain Gaussian distributions with means very close to zero and standard deviations around to 2.5 VEM. The accuracy in the prediction of the muonic signal is shown, this time as a

scatter plot, in Figure 6. The Pearson correlation coefficient is 0.98 for p, He, N and Fe; a truly remarkable level of correlation.

We have carefully checked whether potential biases arise in the estimation of the muonic signal as a function of the following variables: distance of the station to the position of the core at the ground (Figure 7), simulated energy of the event (Figure 8), $\sec\theta$ (Figure 9) and the total signal recorded by every water-Cherenkov detector (Figure 10). For this set of variables, the differences (in absolute value) between true and predicted signals are always below 2 VEM. Relative errors are typically below 10%. Our predictive power does not depend on the energy or the zenith angle of the air shower since the differences between predicted and measured signals are flat as a function of those two variables. At distances close to the core the spread in differences is wider. In addition to the fact that the number of events is smaller at short and very large distances to the shower core, we attribute part of this behaviour to the presence of a stronger contribution of the electromagnetic component.

4.2. EPOS-LHC simulations: results at detector level

In our view, the crucial test our approach must overcome is to prove that, once the learning process has finished and the internal architecture of the net has been fixed using events generated with QGSJETII-04, the capability to accurately estimate the number of muons in a detector is independent of the hadronic model used. With this goal in mind, we generated a sample of events that used EPOS-LHC as the model for hadronic interactions (see Table 1). The results of this exercise are shown in Figures 11–16. These Figures demonstrate that the predictive power of the neural network is good. The relative error stays below 10%, and the absolute difference between predicted and true signal does not exceed 2 VEM units. In addition, no sensible bias occurs as a function of the usual variables previously checked. We interpret this as a sign that the correlations between the observables used in the models under consideration are similar and therefore show a high degree of universality.

5. Conclusions

This work explores how machine learning algorithms help in advancing our understanding of the physics of extensive air showers. Taking as an example the Surface Detector of the Pierre Auger Observatory, we have demonstrated that deep learning methods are a powerful tool to separate the muonic and electromagnetic signals that form the traces registered by the water-Cherenkov detectors of the Auger Surface Detector Array. Based on Monte Carlo studies, we prove that, for each individual station, it is possible to give a proper estimation of the number of recorded muons. We obtain precisions that are typically better than 10%. A remarkable figure when compared to previous attempts to estimate the muonic signal. Our method can be applied to a wide spectrum of primary nuclei, energies, zenith angles and distance ranges. It would be interesting to see how those algorithms

perform when applied to experimental data and how they compare with previous studies that reported a substantial discrepancy in the number of muons measured in data and those predicted by simulations. Combined with the future data provided by AugerPrime, machine learning techniques seem the ideal tool to gain further insight into the mysteries of ultra-high energy cosmic rays.

Acknowledgments

We warmly thank our colleagues of the Pierre Auger Observatory for their support and for letting us use the official software of the collaboration. We sincerely acknowledge many illuminating discussions with M. Erdmann, D. Veberič, A. A. Watson and A. Yushkov.

This work was done under the auspices of MINECO project FPA2015-70420-C2-2-R. C.J. Todero Peixoto's research was developed with the support of the CENAPAD-SP (Centro Nacional de Processamento de Alto Desempenho em São Paulo), project UNICAMP / FINEP - MCT. He also received support through process number: 2016/19764-9, Fundação de Amparo à Pesquisa do Estado de São Paulo (FAPESP).

The authors acknowledge the National Laboratory for Scientific Computing (LNCC/MCTI, Brazil) for providing HPC resources of the SDumont supercomputer, which have contributed to the research results reported in this paper (<http://sdumont.lncc.br>).

References

- [1] J. Linsley, Evidence for a primary cosmic-ray particle with energy 10^{20} -eV, *Phys. Rev. Lett.* 10 (1963) 146–148. doi:10.1103/PhysRevLett.10.146.
- [2] A. Aab, et al., The Pierre Auger Cosmic Ray Observatory, *Nucl. Instrum. Meth. A* 798 (2015) 172–213. arXiv:1502.01323, doi:10.1016/j.nima.2015.06.058.
- [3] A. Aab, et al., Testing Hadronic Interactions at Ultrahigh Energies with Air Showers Measured by the Pierre Auger Observatory, *Phys. Rev. Lett.* 117 (19) (2016) 192001. arXiv:1610.08509, doi:10.1103/PhysRevLett.117.192001.
- [4] A. Aab, et al., Muons in air showers at the Pierre Auger Observatory: Mean number in highly inclined events, *Phys. Rev. D* 91 (3) (2015) 032003, [Erratum: *Phys. Rev. D* 91, no. 5, 059901 (2015)]. arXiv:1408.1421, doi:10.1103/PhysRevD.91.059901, 10.1103/PhysRevD.91.032003.
- [5] A. Aab, et al., The Pierre Auger Observatory Upgrade - Preliminary Design Report arXiv:1604.03637.
- [6] R. U. Abbasi, et al., Study of muons from ultra-high energy cosmic ray air showers measured with the Telescope Array experiment arXiv:1804.03877.
- [7] A. Letessier-Selvon, P. Billoir, M. Blanco, I. C. Mariş, M. Settimo, Layered water Cherenkov detector for the study of ultra high energy cosmic rays, *Nucl. Instrum. Meth. A* 767 (2014) 41–49. arXiv:1405.5699, doi:10.1016/j.nima.2014.08.029.

- [8] J. Schmidhuber, Deep learning in neural networks: An overview, *Neural Networks* 61 (2015) 85–117.
- [9] Y. LeCun, Y. Bengio, G. E. Hinton, Deep learning, *Nature* 521 (7553) (2015) 436–444.
- [10] S. Argiro, S. L. C. Barroso, J. Gonzalez, L. Nellen, T. C. Paul, T. A. Porter, L. Prado, Jr., M. Roth, R. Ulrich, D. Veberic, The Offline Software Framework of the Pierre Auger Observatory, *Nucl. Instrum. Meth. A* 580 (2007) 1485–1496. arXiv:0707.1652, doi:10.1016/j.nima.2007.07.010.
- [11] E. Jones, T. Oliphant, P. Peterson, et al., SciPy: Open source scientific tools for Python (2001).
URL <http://www.scipy.org/>
- [12] F. Pedregosa, G. Varoquaux, A. Gramfort, V. Michel, B. Thirion, O. Grisel, M. Blondel, P. Prettenhofer, R. Weiss, V. Dubourg, J. Vanderplas, A. Passos, D. Cournapeau, M. Brucher, M. Perrot, E. Duchesnay, Scikit-learn: Machine learning in Python, *J. Mach. Learn. Res.* 12 (2011) 2825–2830.
URL <http://dl.acm.org/citation.cfm?id=1953048.2078195>
- [13] F. Chollet, et al., Keras, <https://github.com/keras-team/keras> (2015).
- [14] M. Abadi, P. Barham, J. Chen, Z. Chen, A. Davis, J. Dean, M. Devin, S. Ghemawat, G. Irving, M. Isard, M. Kudlur, J. Levenberg, R. Monga, S. Moore, D. G. Murray, B. Steiner, P. Tucker, V. Vasudevan, P. Warden, M. Wicke, Y. Yu, X. Zheng, Tensorflow: A system for large-scale machine learning, in: *Proceedings of the 12th USENIX Conference on Operating Systems Design and Implementation, OSDI'16*, USENIX Association, Berkeley, CA, USA, 2016, pp. 265–283.
URL <http://dl.acm.org/citation.cfm?id=3026877.3026899>
- [15] I. Goodfellow, Y. Bengio, A. Courville, *Deep Learning*, MIT Press, 2016, <http://www.deeplearningbook.org>.
- [16] V. Nair, G. E. Hinton, Rectified linear units improve restricted Boltzmann machine, in: editor (Ed.), *Proceedings of the 27th International Conference on Machine Learning*, 2010.
- [17] X. Glorot, A. Bordes, Y. Bengio, Deep sparse rectifier neural networks, in: G. Gordon, D. Dunson, M. Dudk (Eds.), *Proceedings of the Fourteenth International Conference on Artificial Intelligence and Statistics*, Vol. 15 of *Proceedings of Machine Learning Research*, PMLR, Fort Lauderdale, FL, USA, 2011, pp. 315–323.
URL <http://proceedings.mlr.press/v15/glorot11a.html>
- [18] D. P. Kingma, J. Ba, Adam: A method for stochastic optimization, *CoRR* abs/1412.6980. arXiv:1412.6980.
URL <http://arxiv.org/abs/1412.6980>

- [19] X. Bertou, et al., Calibration of the surface array of the Pierre Auger Observatory, *Nucl. Instrum. Meth. A*568 (2006) 839–846. doi:10.1016/j.nima.2006.07.066.
- [20] A. Aab, et al., The Pierre Auger Observatory: Contributions to the 35th International Cosmic Ray Conference (ICRC 2017), 2017. arXiv:1708.06592.
- [21] A. Aab, et al., Inferences on mass composition and tests of hadronic interactions from 0.3 to 100 EeV using the water-Cherenkov detectors of the Pierre Auger Observatory, *Phys. Rev. D* 96 (12) (2017) 122003. arXiv:1710.07249, doi:10.1103/PhysRevD.96.122003.
- [22] S. Ostapchenko, Monte Carlo treatment of hadronic interactions in enhanced Pomeron scheme: I. QGSJET-II model, *Phys. Rev. D*83 (2011) 014018. arXiv:1010.1869, doi:10.1103/PhysRevD.83.014018.
- [23] K. Werner, F.-M. Liu, T. Pierog, Parton ladder splitting and the rapidity dependence of transverse momentum spectra in deuteron-gold collisions at RHIC, *Phys. Rev. C*74 (2006) 044902. arXiv:hep-ph/0506232, doi:10.1103/PhysRevC.74.044902.
- [24] D. Heck, J. Knapp, J. Capdevielle, G. Schatz, T. Thouw., A Monte-Carlo code to simulate extensive air showers - Report FZKA 6019, Tech. rep., Forschungszentrum Karlsruhe, <https://www.ikp.kit.edu/corsika/70.php> (1998).

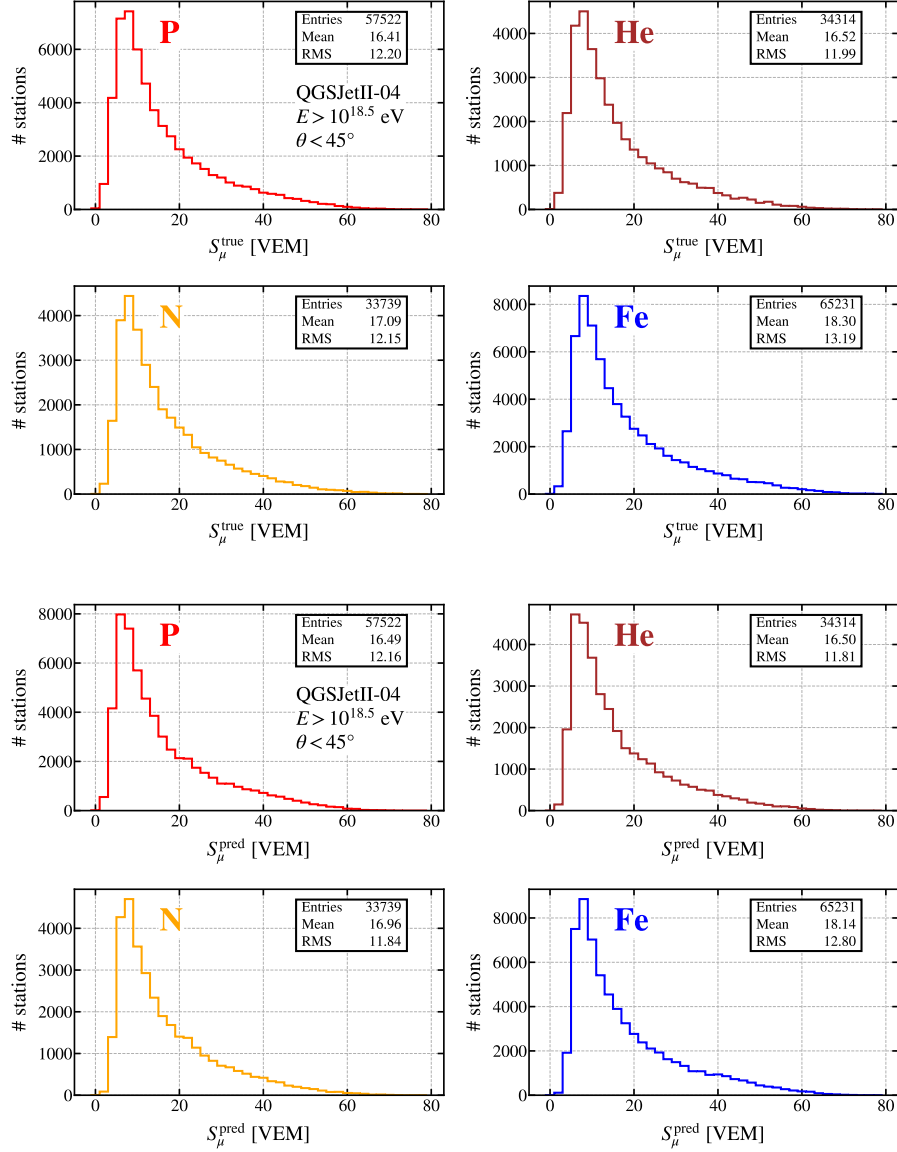


Figure 4: (Four top panels) True muon signals for four different species of primary nuclei. Each entry corresponds to the muonic trace recorded by each individual water-Cherenkov detector. (Four bottom panels) Predicted muon signals using a deep neural network (see text for additional details). The events have been generated in an energy interval that spans from $\log_{10}(E/\text{eV})=18.5$ up to $\log_{10}(E/\text{eV})=20$.

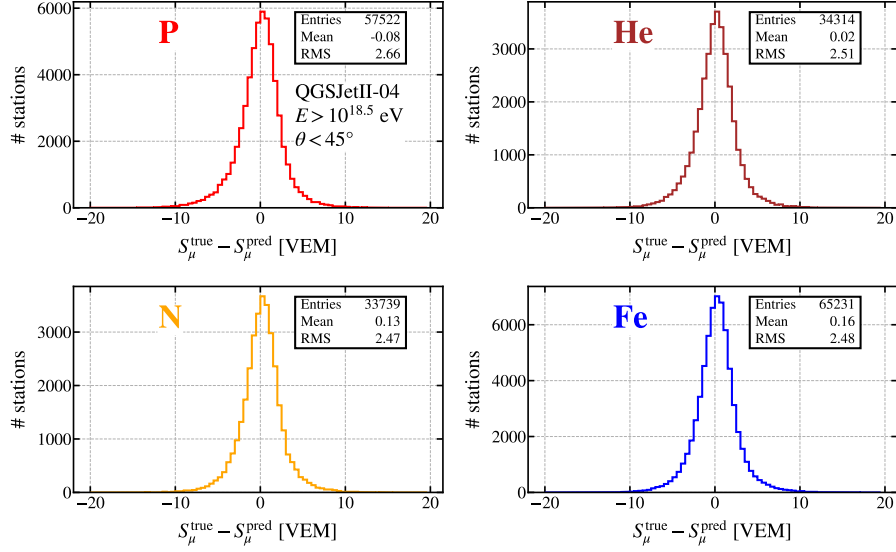


Figure 5: Difference between true and predicted muon signals for four different kinds of primaries. Every entry corresponds to the information provided by a single water-Cherenkov detector.

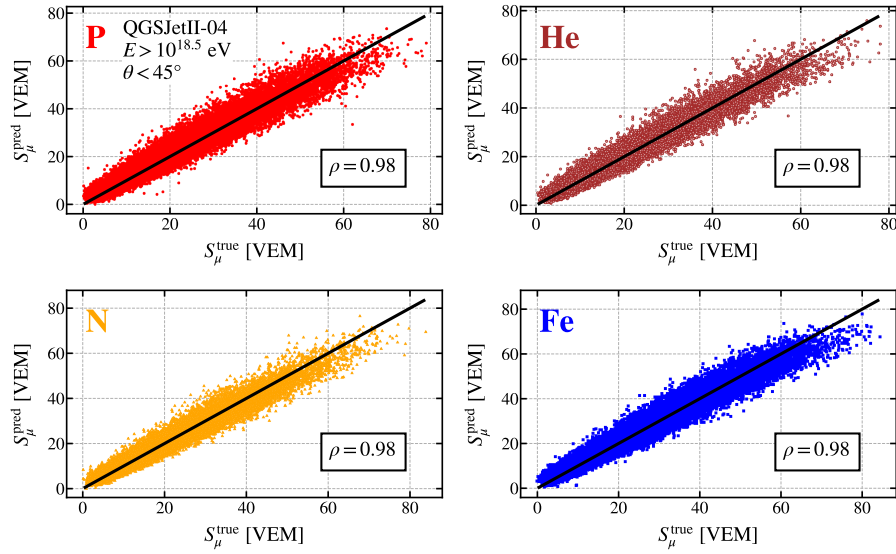


Figure 6: Correlation between the true and the predicted muon signals obtained after building and training a deep neural network.

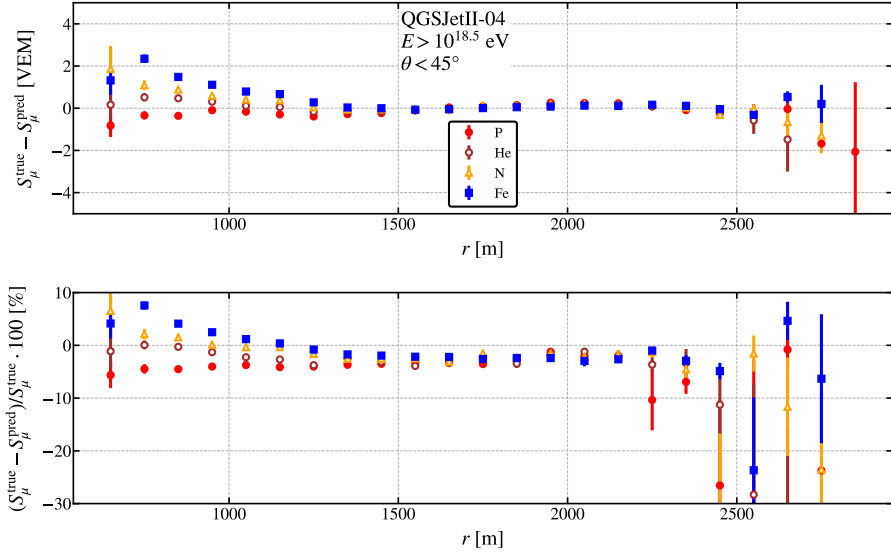


Figure 7: Difference between true and predicted muon signals as a function of the distance to the core (top panel) and its associated relative error (bottom panel).

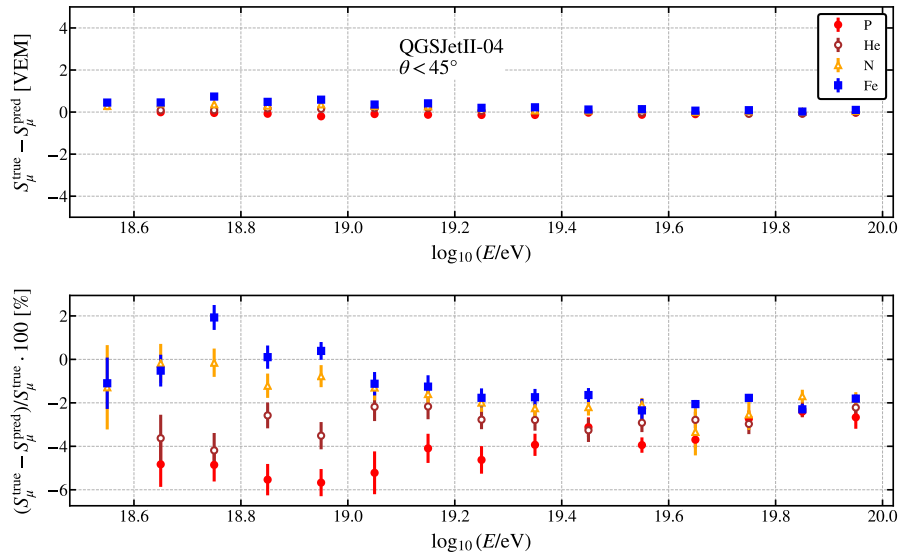


Figure 8: Difference between true and predicted muon signals as a function of the event Monte Carlo energy (top panel) and its associated relative error (bottom panel).

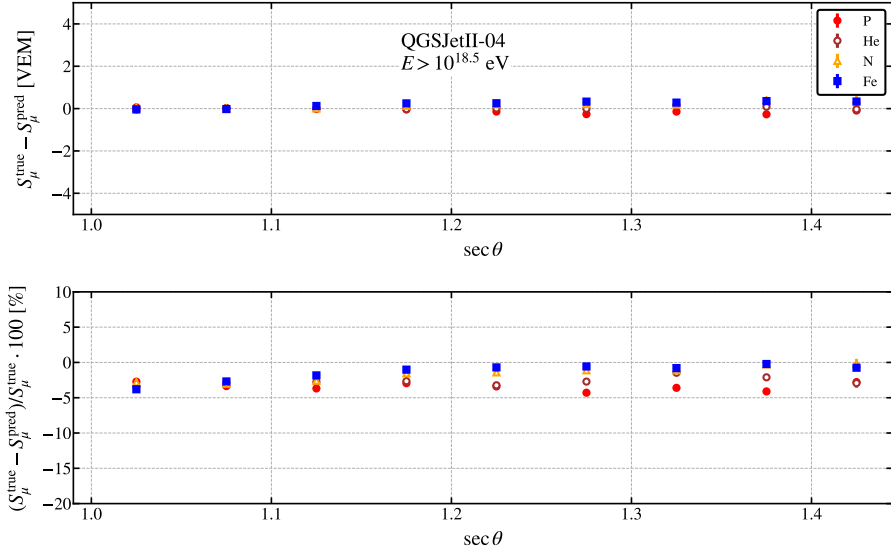


Figure 9: Difference between true and predicted muon signals as a function of $\sec \theta$ (top panel) and its associated relative error (bottom panel).

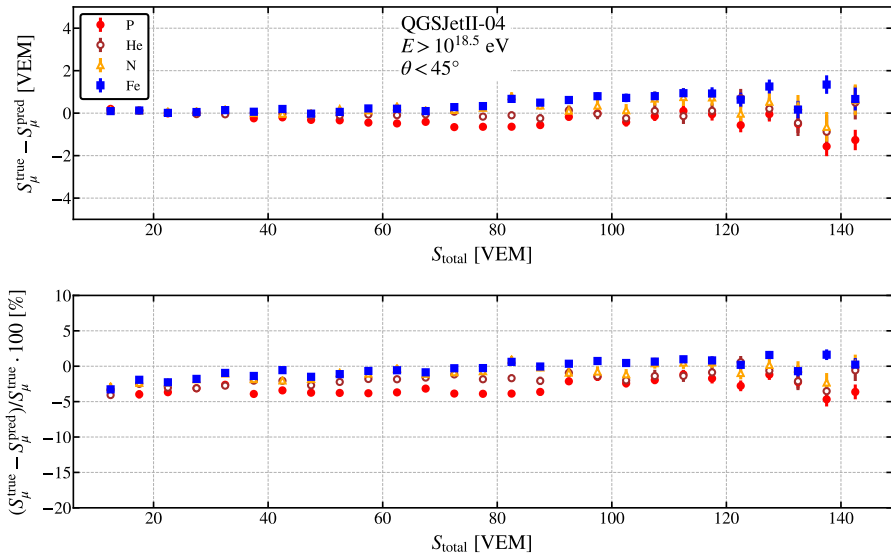


Figure 10: Difference between true and predicted muon signals as a function of the total signal registered in individual stations (top panel) and its associated relative error (bottom panel).

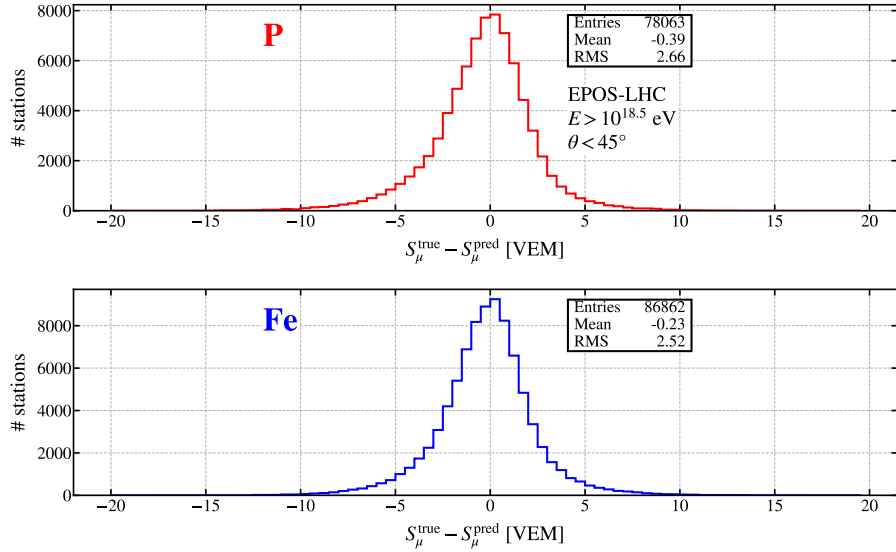


Figure 11: Difference between true and predicted muonic signals at detector level for two different kinds of primaries. Events have been generated using EPOS-LHC to model hadronic interactions.

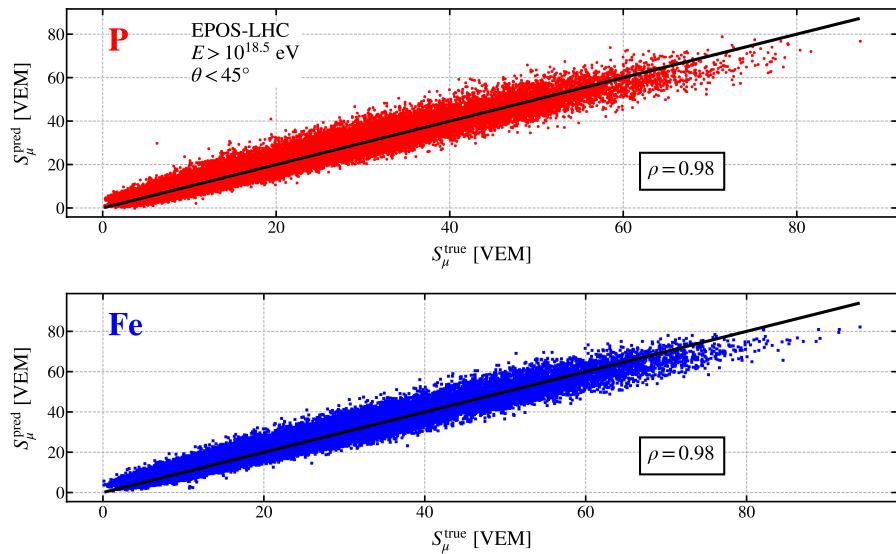


Figure 12: Correlation between the true muon signal and the predicted muon signal. Events have been generated using EPOS-LHC to model hadronic interactions.

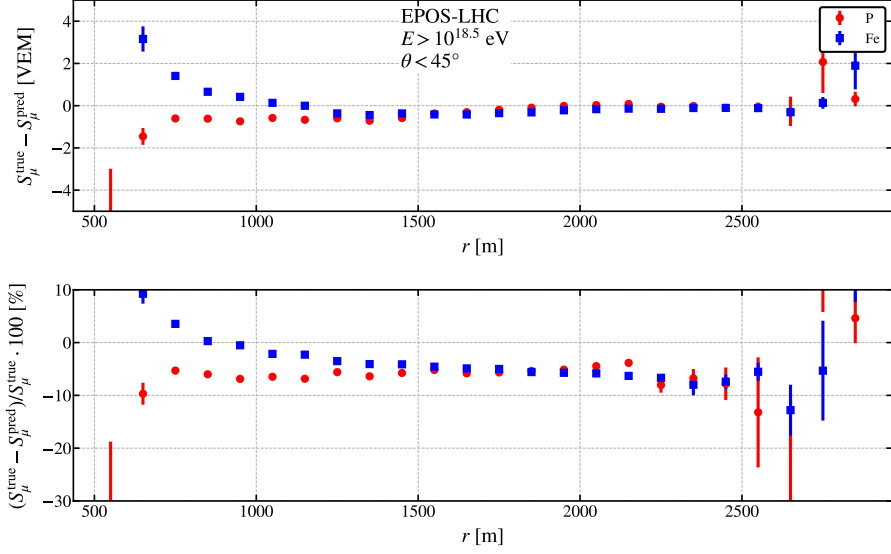


Figure 13: Difference between true and predicted muon signals as a function of the distance to the core (top panel) and its associated relative error (bottom panel). Events have been generated using EPOS-LHC to model hadronic interactions.

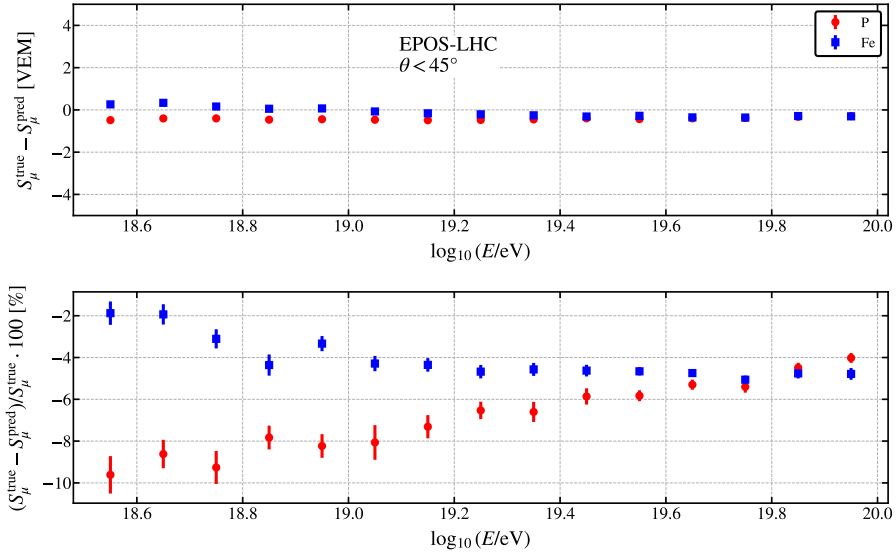


Figure 14: Difference between true and predicted muon signals as a function of the Monte Carlo event energy (top panel) and its associated relative error (bottom panel). Events have been generated using EPOS-LHC to model hadronic interactions.

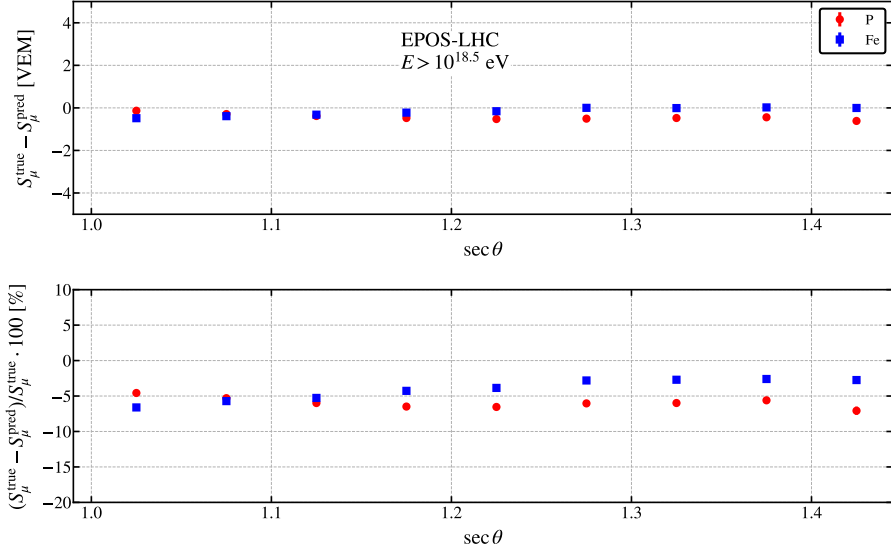


Figure 15: Difference between true and predicted muon signals as a function of $\sec \theta$ (top panel) and its associated relative error (bottom panel). Events have been generated using EPOS-LHC to model hadronic interactions.

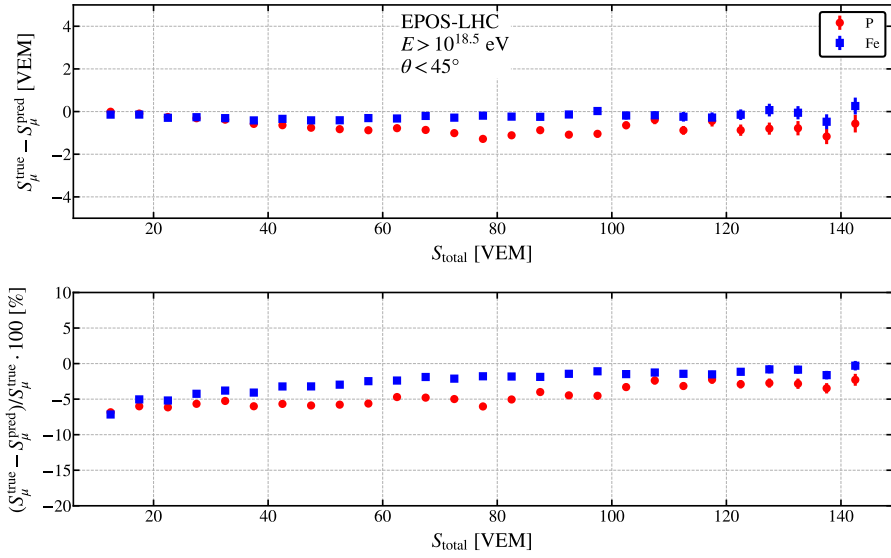


Figure 16: Difference between true and predicted muon signals as a function of the total signal registered in individual stations (top panel) and its associated relative error (bottom panel). Events have been generated using EPOS-LHC to model hadronic interactions.